Chemical Research in Toxicology

Article

pubs.acs.org/crt

Base-Displaced Intercalated Conformation of the 2-Amino-3-methylimidazo[4,5-*f*]quinoline N^2-dG DNA Adduct Positioned at the Nonreiterated G^1 in the *Nar*I Restriction Site

Kallie M. Stavros,[†] Edward K. Hawkins,[‡] Carmelo J. Rizzo,[†] and Michael P. Stone*[,†]

[†]Department of Chemistry, Center in Molecular Toxicology, Vanderbilt-Ingram Cancer Center, and Vanderbilt Institute of Chemical Biology, Vanderbilt University, Nashville, Tennessee 37235-1822, United States

Supporting Information

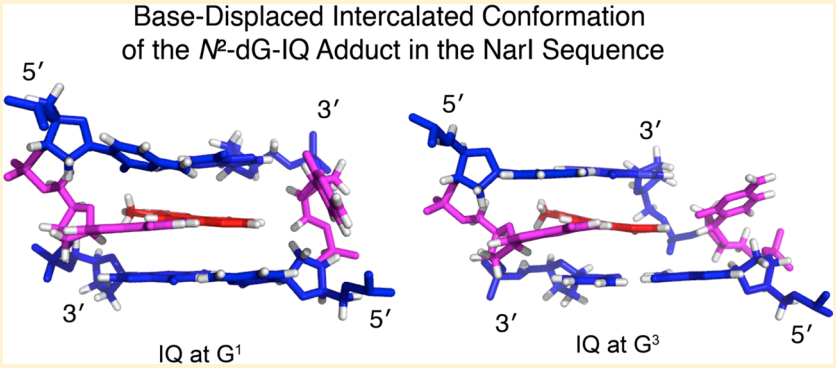

ABSTRACT: The conformation of an N^2-dG adduct arising from the heterocyclic amine 2-amino-3-methylimidazo[4,5-*f*]quinoline (IQ), a potent food mutagen, was determined in 5′-d($C^1T^2C^3\underline{X}^4G^5C^6G^7C^8C^9A^{10}T^{11}C^{12}$)-3′:5′-d($G^{13}A^{14}T^{15}G^{16}G^{17}C^{18}G^{19}C^{20}C^{21}G^{22}A^{23}G^{24}$)-3′; $\underline{X}$ = N^2-dG-IQ, in which the modified nucleotide $\underline{X}^4$ corresponds to G^1 in the 5′-d($G^1G^2CG^3CC$)-3′ *Nar*I restriction endonuclease site. Circular dichroism (CD) revealed blue shifts relative to the unmodified duplex, consistent with adduct-induced twisting, and a hypochromic effect for the IQ absorbance in the near UV region. NMR revealed that the N^2-dG-IQ adduct adopted a base-displaced intercalated conformation in which the modified guanine remained in the *anti* conformation about the glycosidic bond, the IQ moiety intercalated into the duplex, and the complementary base C^{21} was displaced into the major groove. The processing of the N^2-dG-IQ lesion by hpol η is sequence-dependent; when placed at the reiterated G^3 position, but not at the G^1 position, this lesion exhibits a propensity for frameshift replication [Choi, J. Y., et al. (2006) *J. Biol. Chem.*, *281*, 25297−25306]. The structure of the N^2-dG-IQ adduct at the nonreiterated G^1 position was compared to that of the same adduct placed at the G^3 position [Stavros, K. M., et al. (2014) *Nucleic Acids Res.*, *42*, 3450−3463]. CD indicted minimal spectral differences between the G^1 vs G^3 N^2-dG-IQ adducts. NMR indicated that the N^2-dG-IQ adduct exhibited similar base-displaced intercalated conformations at both the G^1 and G^3 positions. This result differed as compared to the corresponding C8-dG-IQ adducts placed at the same positions. The C8-dG-IQ adduct adopted a minor groove conformation when placed at position G^1 but a base-displaced intercalated conformation when placed at position G^3 in the *Nar*I sequence. The present studies suggest that differences in lesion bypass by hpol η may be mediated by differences in the 3′-flanking sequences, perhaps modulating the ability to accommodate transient strand slippage intermediates.

INTRODUCTION

Browning meats during cooking imparts flavor, but it also forms heterocyclic amines (HCAs) such as 2-amino-3-methylimidazo-[4,5-*f*]quinoline (IQ) (Scheme 1).[1−5] IQ is produced in cooking at parts per billion levels.[6,7] It has also been detected in tobacco smoke.[8] IQ induces tumors in rodents and monkeys.[9−12] Liver, forestomach, and lung tumors have been observed in mice,[13] whereas liver, intestine, zymbal gland, clitoral gland, skin,[14] mammary gland, and ear duct tumors have been observed in rats.[15] IQ exhibits TD_{50} values of 0.7 and 14.7 mg/kg/day in rats and mice, respectively.[16] Human exposures, estimated to be 60 ng/day,[17] are likely to contribute to cancer etiology.[18,19] Human exposures to HCAs have been associated with cancers of the pancreas,[20] colon,[21] prostate,[22] and breast.[23,24] HCAs and their metabolites have been isolated from human urine.[25]

IQ is a strong mutagen in *Salmonella typhimurium* reversion (Ames) assays and is active in both point and frameshift tester strains.[3,26,27] It is particularly active in tester strain TA98, which is designed to detect two-nucleotide deletions in a CG repeat sequence. Despite the fact that IQ is formed at lower levels than another HCA, 2-amino-1-methyl-6-phenylimidazo[4,5-*b*]-pyridine (PhIP),[28] it is two orders of magnitude more

Received: April 9, 2015
Published: June 17, 2015

DOI: 10.1021/acs.chemrestox.5b00140
Chem. Res. Toxicol. 2015, 28, 1455−1468

Scheme 1. Bioactivation of IQ[a]

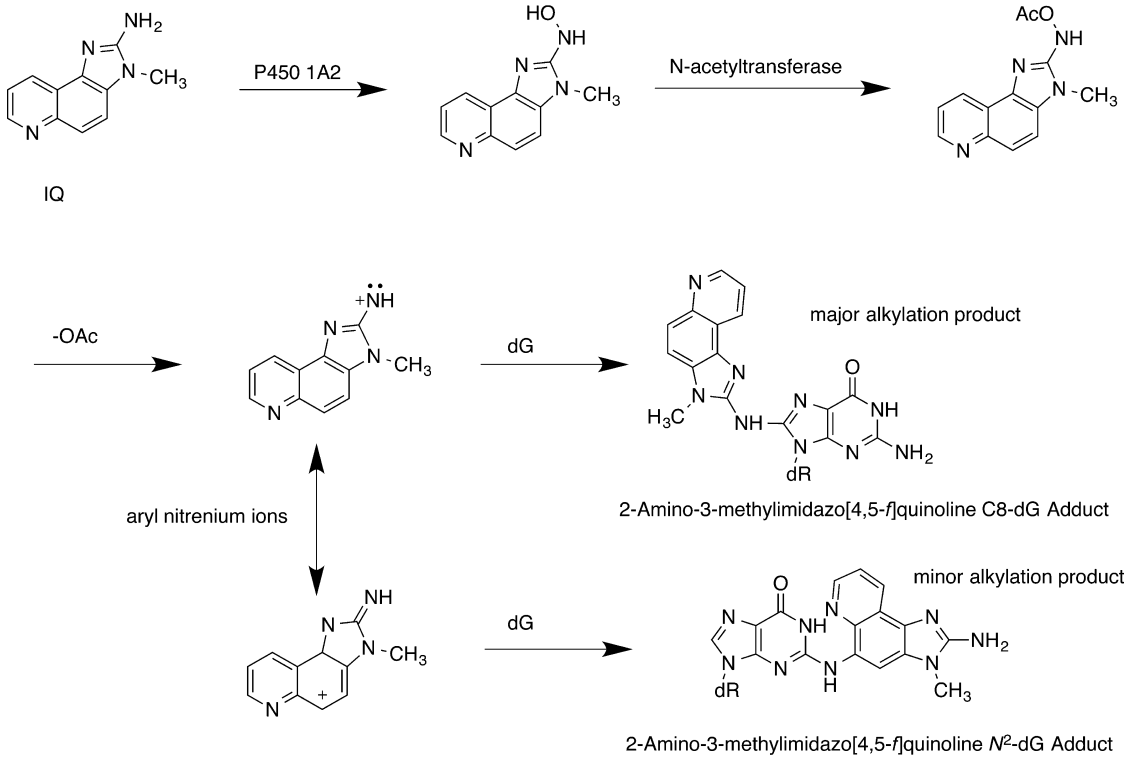

[a]Cytochrome P450-mediated N-hydroxylation followed by N-acetylation of the hydroxylamine and deacetylation forms an electrophilic aryl nitrenium ion. The aryl nitrenium ion alkylates guanine in DNA via the IQ amine nitrogen to form the C8-dG-IQ adduct or, alternatively, alkylates DNA via the C5 position of the IQ ring to form the N^2-dG-IQ adduct.

mutagenic than PhIP in TA98 cells.[3] IQ is also an order of magnitude more mutagenic than that of the mycotoxin, aflatoxin B_1.[18] Consequently, it may play a significant role in mutagenesis. IQ gives rise to mutations at G:C base pairs in *Escherichia coli*[29,30] and induces two-nucleotide frameshifts in CG repeats. The mammalian *hprt*[31] and *ef-2*[32] gene assays reveal similar levels of mutations induced by IQ. In mammalian cells, base pair substitutions predominate.[33−35] Sister chromatid exchange has been observed in rodent cells exposed to IQ.[36−38]

IQ-mediated genotoxicity is primarily derived from CYP P450 oxidation to an *N*-hydroxylamine,[39−43] although extrahepatic CYP P450s have been shown to oxidize HCAs with lower efficiencies (Scheme 1).[44] N-Acetyl transferases, particularly NAT2,[45−47] then acetylate the *N*-hydroxylamine. In humans, the *NAT2* fast acetylator polymorphism has been correlated with increased genotoxicity and cancer.[48−50] Solvolysis of the N-acetoxy intermediate yields the ultimate electrophile, a nitrenium ion.[35,44] This species reacts predominately at C8-dG, while a minor alkylation product is formed at N^2-dG.[51−53] IQ may also be metabolized to a reactive and genotoxic *N*-nitrosamine that exhibits similar regioselectivity with regard to DNA alkylation.[54,55]

Levels of C8- and N^2-dG-IQ adducts have been measured in rat and primate tissues using mass spectrometry.[56,57] Turesky and co-workers[58] monitored C8-dG-IQ adduct formation in human hepatocyte cells using tandem liquid chromatography−electrospray ionization mass spectrometry. Levels ranged from 7 to 26 adducts per 10^7 bases. Although it is less abundant in DNA, the N^2-dG-IQ adduct was more persistent in rat tissues, suggesting that it is repaired less efficiently.[59] Consequently, it has been anticipated that the N^2-dG-IQ adduct may play a significant role in IQ-mediated genotoxicity.

The preparation of phosphoramidite reagents of the C8- and N^2-dG-IQ adducts in which the Buchwald−Hartwig palladium-catalyzed *N*-arylation was the key C−N bonding-forming step,[60−63] allowed site-specific incorporation of these adducts into oligodeoxynucleotides using solid-phase synthesis. Subsequently, the conformation of the N^2-dG-IQ adduct was determined in the 5′-d($C^1T^2C^3G^4G^5C^6\underline{X}^7C^8C^9A^{10}T^{11}C^{12}$)-3′:5′-d($G^{13}A^{14}T^{15}G^{16}G^{17}C^{18}G^{19}C^{20}C^{21}G^{22}A^{23}G^{24}$)-3′ duplex; $\underline{X}$ = N^2-dG-IQ.[64] This duplex contained the recognition sequence of the *Nar*I restriction endonuclease, 5′-d($CG^1G^2CX^3CC$)-3′, in which X^3 in the *Nar*I sequence corresponds to X^7 in this dodecamer. When placed at the X^7 position, the IQ moiety intercalated, with the IQ H4a and CH_3 protons facing the minor groove and the IQ H7a, H8a, and H9a protons facing the major groove. The adducted nucleotide maintained the *anti* conformation about the glycosidic bond. The complementary dC was extruded into the major groove. The duplex maintained its thermal stability, which was attributed, in part, to stacking between the IQ heterocyclic ring and the 5′- and 3′-neighboring base pairs. The base-displaced intercalated conformation of the N^2-dG-IQ adduct differed from that of the C8-dG-IQ adduct,[65] providing insight as to the persistence of the N^2-dG-IQ adduct[59] and its processing during replication and repair.

The *Nar*I sequence, 5′-d($G^1G^2CG^3CC$)-3′, provides a platform for investigating sequence-specific perturbation of DNA conformation by IQ adducts, in relationship to biological processing.[66−71] In bacterial systems, the G^3 position is a hot spot for two-base frameshift deletions, whereas the G^1 position

DOI: 10.1021/acs.chemrestox.5b00140
Chem. Res. Toxicol. 2015, 28, 1455−1468

is not.[67−69,71] As well, Choi et al.[72] showed that the human DNA polymerase (hpol) η produces two-base deletions when replicating past the N^2-dG-IQ adduct located at position G^3, but it does not when located at position G^1, *in vitro*.

Presently, in an effort to understand how sequence context in the *Nar*I restriction site modulates the processing of N^2-dG-IQ adducts, the N^2-dG-IQ adduct has been incorporated into 5′-d($C^1T^2C^3\underline{X}^4G^5C^6G^7C^8C^9A^{10}T^{11}C^{12}$)-3′:5′-d($G^{13}A^{14}T^{15}G^{16}G^{17}C^{18}G^{19}C^{20}C^{21}G^{22}A^{23}G^{24}$)-3′; $\underline{X}$ = N^2-dG-IQ, in which the modified nucleotide $\underline{X}^4$ corresponds to G^1 in the *Nar*I sequence (Chart 1). The conformation of the N^2-dG-IQ adduct in this duplex, as determined by NMR spectroscopy, is similar to its conformation at the $\underline{X}^7$ position (the G^3 position of the *Nar*I sequence).[64] The IQ heterocyclic ring forms a base-displaced intercalated conformation, disrupting Watson−Crick hydrogen bonding at the lesion site, and flips the complementary cytosine into the major groove. Thus, the N^2-dG-IQ adduct favors a base-displaced intercalated conformation at both positions G^1 and G^3 of the *Nar*I sequence. Small changes in the two base-displaced intercalated conformations at the G^1 vs G^3 positions, and differences in their biological processing, e.g., by hpolη, may be due to differences in the respective 3′-flanking sequences, the importance of which have been previously noted by Cho and co-workers.[73−75] The sequence-dependent conformational behavior of the N^2-dG-IQ adduct differs from that of the C8-dG-IQ adduct, which favors the base-displaced intercalated conformation when placed at position G^3,[65] but it orients in the minor groove when placed at positions G^1 or G^2.[76]

Chart 1. (A) Structure of 2-Amino-3-methylimidazo[4,5-*f*]quinoline (IQ), (B) Structure of the N^2-dG-IQ Adduct, Showing the Numbering of Guanine Base and IQ Protons, and (C) The Duplex Containing the *Nar*I Sequence, Showing the Numbering of the Nucleotides[a]

A

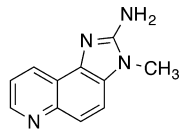

2-Amino-3-methylimidazo[4,5-*f*]quinoline (IQ)

B

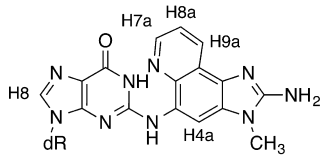

2-Amino-3-methylimidazo[4,5-*f*]quinoline N^2-dG Adduct

C

5′-C^1 T^2 C^3 X^4 G^5 C^6 G^7 C^8 C^9 $A^{10}T^{11}C^{12}$-3′
3′-$G^{24}A^{23}G^{22}C^{21}C^{20}G^{19}C^{18}G^{17}G^{16}T^{15}A^{14}G^{13}$-5′

*Nar*I Oligodeoxynucleotide Sequence

[a]The N^2-dG-IQ adduct is positioned at X^4, which corresponds to the G^1 non-reiterated position of the *Nar*I sequence.

MATERIALS AND METHODS

Sample Preparation. The synthesis of the N^2-dG-IQ-adducted oligodeoxynucleotide, 5′-d(CTC$\underline{X}$GCGCCATC)-3′, has been described.[63] The oligodeoxynucleotide 5′-d(GATGGCGCCGAG)-3′, purified by anion exchange chromatography, was obtained from the Midland Certified Reagent Company (Midland, TX). The oligodeoxynucleotides were purified by HPLC using an acetonitrile gradient from 5 to 12% over 35 min in ammonium formate (pH 7) with a base-deactivated C18 Supesilco LS-18-DB column (Sigma-Aldrich, St. Louis, MO). The oligodeoxynucleotides were characterized MALDI-TOF mass spectrometry in the negative ion mode using a hydroxypicolinic acid matrix. The oligodeoxynucleotides were annealed in 180 μL of 0.1 M NaCl, 0.05 mM Na_2EDTA, and 10 mM NaH_2PO_4 (pH 7.0).

Thermal Melting Experiments. UV thermal melting data were collected on Cary 100 Bio UV spectrometer using 0.5 OD of duplex in 1 mL of solution containing 0.1 M NaCl, 10 mM NaH_2PO_4, and 0.05 mM Na_2EDTA (pH 7.0). The temperature was increased from 25 to 75 °C at a rate of 1 °C/min. The T_m values were calculated from first-derivative analyses of the resulting plots.

Circular Dichroism. The samples contained 0.5 A_{260} units of duplex in 800 μL of 0.1 M NaCl, 0.05 mM Na_2EDTA, and 10 mM Na_2HPO_4 (pH 7.0). Data was obtained by signal averaging on a Jasco 720 spectropolarimeter (Jasco, Inc., Easton, MD) with a response time of 1 s, a scan rate of 20 nm/min, and step resolution of 1 nm across a wavelength of 210−400 nm. Ten scans were signal-averaged.

NMR. Spectra were obtained at 900 MHz using a 5 mm cryogenic probe (Bruker Biospin Inc., Billerica, MA). Oligodeoxynucleotides were prepared at a duplex concentration of 78 nM in 180 μL of 100 mM NaCl, 50 μM Na_2EDTA, in 10 mM Na_2HPO_4 (pH 7.0). To observe nonexchangeable protons samples were exchanged with D_2O and dissolved in 180 μL of 99.996% D_2O. NOESY[77] spectra were collected at 150, 200, or 250 ms mixing times and relaxation delay of 1.8 s, using TPPI quadrature detection. Data were recorded with 2K real points in the *t2* dimension and 512 real points in the *t1* dimension. Spectra were zero-filled during processing to create a 2K × 2K matrix. The temperature was 15 °C. To observe exchangeable protons, samples were prepared in 9:1 H_2O/D_2O. Water suppression was achieved by the Watergate pulse sequence.[78] NOESY spectra were collected at 5 °C with a 100 ms mixing time and a relaxation delay of 1.2 s. Chemical shifts were referenced to the chemical shift of water at the corresponding temperature, with respect to trimethylsilyl propanoic acid (TSP). Data were processed with TOPSPIN (2.0.b.6, Bruker Biospin Inc., Billerica, MA).

NMR Experimental Restraints. The spectral data were evaluated using the program SPARKY.[79] The intensities of NOE cross-peaks were measured by volume integrations. The bounds for overlapped peaks were optimized manually. Noise was assigned half the intensity of the weakest peak, and motion was assumed to be isotropic. The integrated intensities of the cross-peaks were combined with calculated intensities generated from complete relaxation matrix analysis of the starting DNA structure to generate a hybrid intensity matrix.[80,81] The program MARDIGRAS,[82−84] using the RANDMARDI[84,85] algorithm, was used to refine the hybrid matrix by iteration between the calculated and experimental NOE intensities, yielding calculated interproton distances. The calculations were initiated using isotropic correlation times of 2, 3, and 4 ns. Analysis of these calculated interproton distances yielded experimental distance restraints used in subsequent molecular dynamics calculations.

Restrained Molecular Dynamics Calculations. A starting structure in which G^4 in the B-type DNA duplex[86] was replaced by the N^2-dG-IQ adduct was built in InsightII (Accelrys Inc., San Diego, CA). Partial charges for the modified base were calculated in GAUSSIAN[87] using the basis set B3LYP/6-31G*.[64] The starting

DOI: 10.1021/acs.chemrestox.5b00140
Chem. Res. Toxicol. 2015, 28, 1455−1468

structure was energy-minimized for 1000 cycles using the steepest descent method. The generalized Born model[88] with parameters developed by Tsui and Case[89] was used for implicit water simulation. rMD calculations with a simulated annealing protocol using 0.1 M salt were run using AMBER 10[90] and the parm99[91] force field. A force constant of 32 kcal mol^{-1} $Å^{-2}$ was applied to all restraints. A simulated annealing protocol[92] coupled the molecule to a heat bath was used for temperature control. The system was heated to 600 K in 1 ps, held for 1 ps, cooled to 100 K in 16 ps, and then cooled to 0 K in 2 ps using an 18 Å cutoff. Data were recorded every picosecond. Further refinement was performed using a longer 100 ps (100 000 steps) protocol. Here, the temperature was increased from 0 to 600 K during steps 0 to 5000 with a coupling of 0.5 steps. The temperature was held at 600 K from steps 5001 to 10 000. The system was then cooled from 600 to 100 K over steps 10 001 to 90 000 with a coupling of 4 ps. The system was cooled to 0 K from steps 90 001 to 100 000 with a coupling of 1 ps. Structure coordinates were energy-minimized and saved after each calculation. Nine refined structures were used to create an average structure determined by the lowest deviation from experimental intensities. The average structure was subjected to potential energy minimization using the conjugate gradients method. Theoretical NMR intensities for the calculated structure were determined using CORMA.[80,81] Calculations were run until sixth root residuals (R_1^* values) for NOE intensities of the individual bases as well as the overall residuals for the duplex were below 10%. Helicoidal analysis on the average structure was performed using the CURVES+ web server.[93,94]

RESULTS

Sample Preparation and Characterization. The N^2-dG-IQ adduct was incorporated into 5′-d(CTCXGCGCCATC)-3′ using automated solid-phase synthesis.[63] It was located at position X^4, corresponding to position G^1 in the *Nar*I sequence (Chart 1). The modified oligodeoxynucleotide was purified by C18 reverse-phase HPLC and characterized by MALDI-TOF mass spectrometry in negative ion mode (modified strand *m/z* obsvd, 3779; calcd, 3778; complementary strand *m/z* obsvd, 3712; calcd, 3711). Thermal melting (T_m) profiles of 0.5 A_{260} units of the IQ-modified duplex were monitored at 100 mM NaCl (1 mL volume) as a function of temperature by absorbance at 260 nm. An unmodified duplex was evaluated under the same conditions to provide a basis for comparison. The T_m of the modified duplex was 62 °C, compared to the unmodified duplex, which had a melting temperature of 63 °C. Thus, the N^2-dG-IQ adduct did not greatly reduce the thermal stability of this oligodeoxynucleotide duplex. This result was similar to that observed for the N^2-dG-IQ adduct located at position G^3 (T_m 63 °C) (Table S1, Supporting Information).[64]

Circular Dichroism. The G^1 and G^3 N^2-dG-IQ adducts exhibited maximum UV intensities at 270 nm (Figure 1). In the CD spectrum, a blue shift of 5 nm relative to the unmodified duplex was observed. Below 260 nm, the CD of the G^1 and G^3 N^2-dG-IQ modified duplexes were similar to that of the unmodified duplex. The sign of the molar ellipticity inverted at 260 and 264 nm, respectively, for the G^1 and G^3 adducts, and each exhibited spectral minima at 248 nm, as compared to the unmodified duplex, for which the sign of the molar ellipticity inverted at 261 nm and which exhibited a spectral minima at 248 nm. However, the magnitudes of the molar ellipticities of the G^1 and G^3 adducts were reduced with respect to those of the unmodified *Nar*I duplex. For the C8-dG-IQ single-stranded sample, the IQ-induced circular dichroic signal was reported at 300−360 nm,[61] although it was broad. For the N^2-dG-IQ adducted samples, there was negligible circular dichroic signal detected in this range. Likewise, the UV absorption spectrum was null in this range.

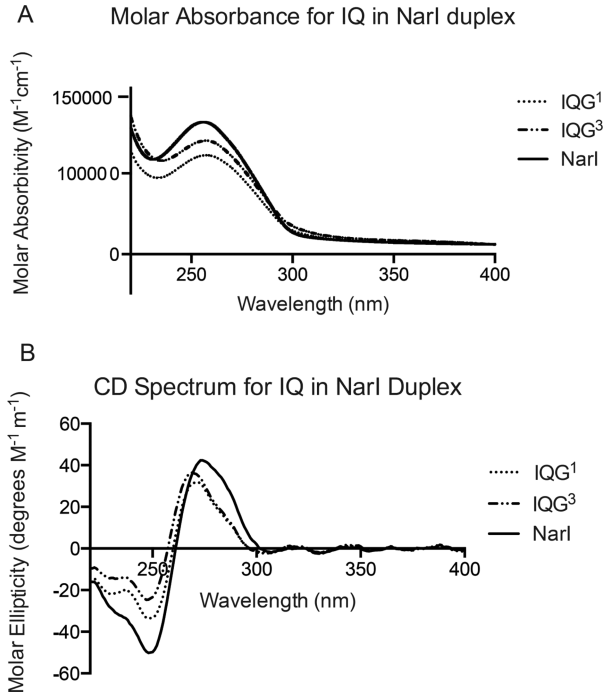

Figure 1. CD spectra for the N^2-dG-IQ adduct when positioned at G^1 or G^3 as compared to the CD spectrum of the unmodified *Nar*I sequence.

NMR. *Assignments of Nonexchangeable DNA Protons.* At 15 °C, the N^2-dG-IQ duplex yielded sharp, well-resolved resonances for nonexchangeable protons (Figure 2). The assignments were made according to established procedures.[95,96] A complete set of sequential NOEs was observed for both the modified strand and the complementary strand. At the modified X^4 base, the sequential X^4 H8 to X^4 H1′ NOE was of similar intensity to that of the other purine H8 to H1′ NOEs. In the complementary strand, at the C^{21} base pair, the sequential C^{21} H1′ to G^{22} H8 NOE was weak, suggesting that the presence of the N^2-dG-IQ lesion resulted in a greater distance between these protons in the complementary strand. The G^7 H8 and G^{19} H8 resonances severely overlapped over the temperature range that the NOESY data were collected. However, base pairs C^6:G^{19} and G^7:C^{18} are two and three base pairs removed from the adduct site in the 3′-direction, and their chemical shifts were within ±0.05 ppm of the G^7 H8 and G^{19} H8 resonances in the unmodified duplex, suggesting that these base pairs were largely unaffected by the presence of the N^2-dG-IQ adduct. With the assignments of the deoxyribose H1′ resonances in hand, the deoxyribose H2′, H2″, H3′, and most of the H4′ resonances could be assigned unequivocally. The stereotopic assignments of the H5′ and H5″ protons were not completed. The assignments of the nonexchangeable protons are tabulated in Table S2 of the Supporting Information.

Exchangeable Protons. Figure 3 shows an expansion of the far downfield region of the NOESY spectrum, showing NOEs between the Watson−Crick imino protons and the amino protons at 5 °C. With the exception of the modified X^4:C^{21} base pair, all protons involved in Watson−Crick hydrogen bonding were observed. At the modified X^4:C^{21} base pair, the X^4 N1H imino proton resonance was identified at 11.8 ppm, but it was nearly completely broadened at 10 °C. The C^{21} N^4 H amino protons were not observed. The broadening of the X^4 N1H proton and the failure to observe the C^{21} N4H protons

DOI: 10.1021/acs.chemrestox.5b00140
Chem. Res. Toxicol. 2015, 28, 1455−1468

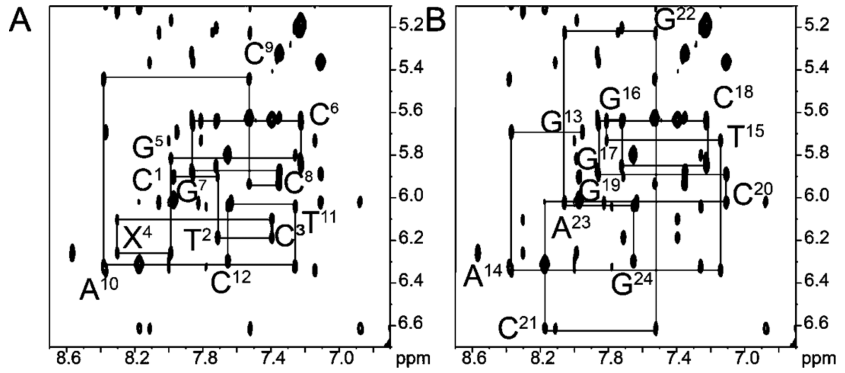

Figure 2. Expanded region of the NOESY spectrum showing NOE connectivity between base aromatic protons and deoxyribose anomeric protons for the N^2-dG-IQ adduct located at the G^1 position of the *Nar*I restriction sequence. (A) Bases C^1–C^{12} of the modified strand. (B) Bases G^{13}–G^{24} of the complementary strand. The spectrum was acquired at 900 MHz with a NOE mixing time of 150 ms. The temperature was 15 °C.

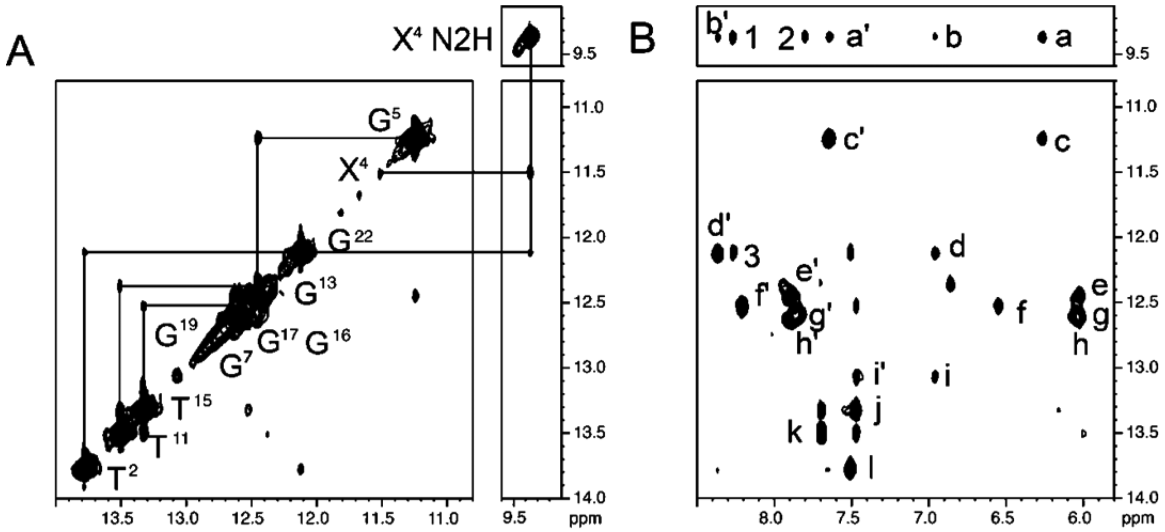

Figure 3. Expanded region of the NOESY spectrum showing the exchangeable proton assignments for the N^2-dG-IQ modified duplex at position G^1 of the *Nar*I restriction sequence. (A) Sequential connectivity of imino protons T^2–T^{11}. (B) NOE connectivity from imino protons to amino protons involved in Watson–Crick hydrogen bonding. The cross-peaks are labeled a′, X^4 N^2H → C^{20} N^4Hb; a, X^4 N^2H → C^{20} N^4Ha; b′, X^4 N^2H → C^3 N^4Hb; b, X^4 N^2H → C^3 N^4Ha; c′, G^5 N1H → C^{20} N^4Hb; c, G^5 N1H → C^{20} N^4Ha; d′, G^{22} N1H → C^3 N^4Hb; e′, G^{19} N1H → C^6 N^4Hb; e, G^{19} N1H → C^6 N^4Ha; f′, G^{16} N1H → C^9 N^4Hb; f, G^{16} N1H → C^9 N^4Ha; g′, G^{17} N1H → C^8 N^4Hb; g, G^{17} → C^8 N^4Ha; h′, G^7 N1H → C^{18} N^4Hb; h, G^7 N1H → C^{18} N^4Ha; i′, G^{24} N1H → C^1 N^4Hb; i, G^{24} N1H → C^1 N^4Ha; j, T^{15} N3H → A^{10} H2; k, T^{11} N3H → A^{14} H2; l, T^2 N3H → A^{23} H2; 1, X^4 N^2H → IQ H4a; 2, X^4 N^2H → IQ H9a; 3, G^{22} N^2H → IQ H4a. The spectrum was acquired in 90:10 H_2O:D_2O at 900 MHz with a NOE mixing time of 150 ms. The temperature was 15 °C.

were attributed to their rapid exchange with water. It exhibited a 1.6 ppm upfield shift as compared to the G^4 N1H resonance in the unmodified duplex, which indicated that it was not involved in Watson–Crick hydrogen bonding. The X^4 N1H proton did not show NOE cross-peaks to the C^{21} N^4H amino protons. However, the X^4 N1H proton exhibited a weak NOE to the X^4 N^2 H amino proton of the modified X^4:C^{21} base pair, observed as a sharp resonance at 9.5 ppm. The X^4 N^2H proton did not exhibit NOEs to the imino protons of the flanking C^3:G^{22} or G^5:C^{20} base pairs; however, it did exhibit NOEs to the C^3 N^4 amino protons of the 5′-flanking C^3:G^{22} base pair as well as IQ protons H4a and H9a. The X^4 N^2H resonance remained sharp to a temperature of 55 °C, which was attributed to the potential for hydrogen bond formation with the nitrogen atom in the IQ ring. No cross-peaks corresponding to the C^{21} N^4H amino protons were observed, suggesting that the C^{21} exocyclic amine was likely solvent-exposed (Figure 3). The assignments of the exchangeable protons are tabulated in Table S3 of the Supporting Information.

IQ Protons. The assignment of the IQ adduct protons is shown in Figure 4. A strong NOE was observed between the IQ H4a proton, observed at 8.57 ppm, with the IQ CH_3 protons, observed as a singlet of area three protons, at 3.23 ppm. The IQ H8a (6.9 ppm) and H9a (7.75 ppm) protons were identified on the basis of their scalar coupling interaction. The IQ H7a resonance (8.11 ppm) was assigned on the basis of its NOE to the IQ H8a proton. In the COSY spectrum, the scalar coupling cross-peak between the IQ H7a and H8a protons was broadened, so the coupling constant could not be determined. This was also observed in NMR spectra of the modified nucleoside[97] and had been observed for the N^2-dG-IQ adduct positioned at G^3 of the *Nar*I sequence.[64] It was attributed to the presence of the quinoline nitrogen atom adjacent to C7 in the IQ ring. The assignments of the IQ protons are tabulated in Table S4 of the Supporting Information.

NOEs between IQ Protons and DNA Protons. A total of 26 NOEs were observed between IQ protons and DNA

DOI: 10.1021/acs.chemrestox.5b00140
Chem. Res. Toxicol. 2015, 28, 1455–1468

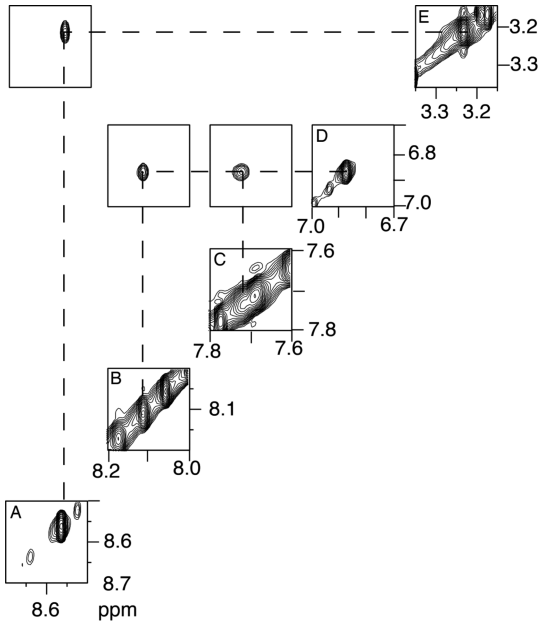

Figure 4. Expanded region of the NOESY spectrum showing the assignments of the IQ aryl ring for the N^2-dG-IQ adduct located at position G^1 of the *Nar*I restriction sequence. (A) The IQ H4a proton resonance was observed at 8.56 ppm. (B) The IQ H7a resonance was observed at 8.11 ppm. (C) The IQ H9a resonance was observed at 7.74 ppm. (D) The IQ H8a resonance was observed at 6.87 ppm. (E) The IQ CH_3 resonance was observed at 3.23 ppm. The spectrum was acquired at 900 MHz with a NOE mixing time of 150 ms. The temperature was 15 °C.

protons (Figure 5). The pattern of NOEs for the IQ CH_3 and H4a protons differed from that of the IQ H7a, H8a, and H9a

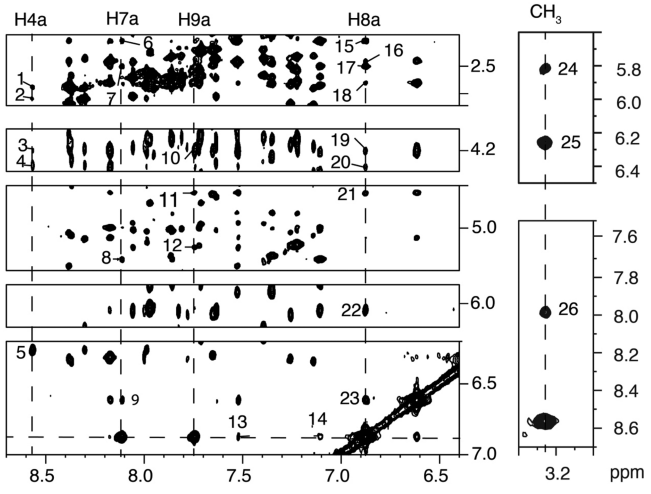

Figure 5. Expansion of the NOESY spectrum showing NOEs between the N^2-dG-IQ adduct located at position G1 of the *Nar*I restriction sequence and the DNA. The peaks are numbered as 1, H4a → X^4 H2″; 2, H4a → X^4 H2′; 3, H4a → X^4 H5′; 4, H4a → X^4 H5″; 5, H4a → X^4 H1′; 6, H7a → C^{20} H2′; 7, H7a → C^{20} H2″; 8, H7a → C^{20} H5; 9, H7a → C^{20} H1′; 10, H9a → G^{22} H5′; 11, H9a → G^{22} H5″; 12, H9a → G^{22} H1′; 13, H8a → G^{22} H8; 14, H8a → C^{20} H6; 15, H8a → C^{20} H2′; 16, H8a → C^{21} H2′; 17, H8a → C^{20} H2″; 18, H8a → C^{21} H2″; 19, H8a → C^{21} H5′; 20, H8a → C^{21} H5″; 21, H8a → C^{21} H4′; 22, H8a → C^{20} H1′; 23, H8a → C^{21} H1′; 24, CH_3 → G^5 H1′; 25, CH_3 → X^4 H1′; 26, CH_3 → G^5 H8. The spectrum was acquired at 900 MHz with a NOE mixing time of 150 ms. The temperature was 15 °C.

protons. The IQ CH_3 and H4a protons exhibited NOEs to the X^4 and G^5 protons in the modified strand. The CH_3 protons showed a strong NOE to X^4 H1′ and a medium NOE to G^5 H8. Weaker NOEs were observed to X^4 H2′, X^4 H2″ (not shown in Figure 5), and G^5 H1′. The H4a proton showed a strong NOE to X^4 H1′ and additional NOEs to X^4 H2′, H2″, and X^4 H5′, H5″. In contrast, the IQ H7a, H8a, and H9a protons exhibited NOEs to protons in the complementary strand. The H7a proton showed a medium NOE to C^{21} H1′ and weak NOEs to C^{20} H5 and C^{20} H2′, H2″. The IQ H8a proton exhibited medium intensity NOEs to C^{20} H1′, H2′, H2″, and C^{21} H1′, and weak NOEs to C^{21} H2′, H2″, and H5′, H5″. There were also weak NOEs between the IQ H8 proton and C^{20} H6 and G^{22} H8. The IQ H9a proton showed a medium NOE to C^{21} H1′ and a weak NOE to C^{20} H2″, as well as weak NOEs to G^{22} H1′, G^{22} H5′, H5″ and weak NOEs to G^{22} H8 and C^{20} H6 and H6. There were no NOEs observed between the IQ protons and either C^{21} H5 or H6. The NOEs between the IQ moiety and the DNA are summarized in Table 1.

Table 1. NOEs from IQ Protons of the N^2-dG-IQ Adduct at Position G^1 of the *Nar*I Restriction Site to Oligodeoxynucleotide Protons and Relative Intensities of the Cross-Peaks

IQ proton	NOEs to oligodeoxynucleotide protons
CH_3	X^4 H1′, strong; G^5 H8, medium; G^5 H1′, weak
H4a	X^4 H1′, strong; X^4 H2″, weak; X^4 H2′, weak; X^4 H5″, weak
H7a	C^{21} H1′, medium; C^{20} H5, medium; C^{20} H2″, weak; C^{20} H2′, weak
H8a	C^{21} H1′, medium; C^{20} H1′, medium; C^{21} H4′, medium; C^{20} H2″, medium; G^{22} H8, weak; C^{20} H6, weak; C^{21} H2′, weak; C^{21} H2″, weak; C^{21} H5′, weak; C^{21} H5″, weak
H9a	C^{21} H1′, medium; C^{20} H5, medium; C^{20} H2″, weak; G^{22} H1′, weak

Chemical Shift Effects. Significant chemical shift perturbations were observed at modified base pair X^4:C^{21} and flanking base pairs C^3:G^{22} and G^5:C^{20} (Figure 6). At modified base pair X^4:C^{21}, the X^4 H8 resonance was shifted downfield 0.47 ppm and the X^4 H1′ resonance was shifted downfield by 0.74 ppm, relative to the unmodified duplex. The C^{21} H6 and H1′ resonances of the complementary base C^{21} were shifted downfield by 0.81 and 1.26 ppm, respectively. At the 5′-neighbor C^3:G^{22} base pair, the C^3 H1′ and H6 resonances were shifted 0.51 and 0.46 ppm downfield, respectively, whereas the G^{22} H1′ and H8 resonances were shifted 0.17 and 0.34 ppm downfield, respectively. At the 3′-neighbor base pair G^5:C^{20}, the G^5 H8 resonance was shifted 0.28 downfield, whereas the C^{20} H6 resonance was shifted 0.19 ppm upfield. The chemical shifts of the other base pairs were relatively unaffected by the presence of the N^2-dG-IQ lesion, shifting less than 0.1 ppm as compared to the unmodified duplex. The relative pattern of chemical shift perturbations closely resembled that of the N^2-dG-IQ adduct located at position G^7.[64] In both instances, the cytosine complementary to the adduct, C^{21} in the present instance and C^{18} when the N^2-dG-IQ adduct was located at position G^7, exhibited the largest downfield shifts, whereas chemical shift perturbations to the bases to either side of the opposite bases were less than half the magnitude of the base directly opposite, either C^{18} or C^{21} for G^3 and G^1. The N^2-dG-IQ H8 proton was shifted downfield as well by 0.4 ppm, and the base protons flanking the modification were also perturbed by a similar magnitude.

DOI: 10.1021/acs.chemrestox.5b00140
Chem. Res. Toxicol. 2015, 28, 1455−1468

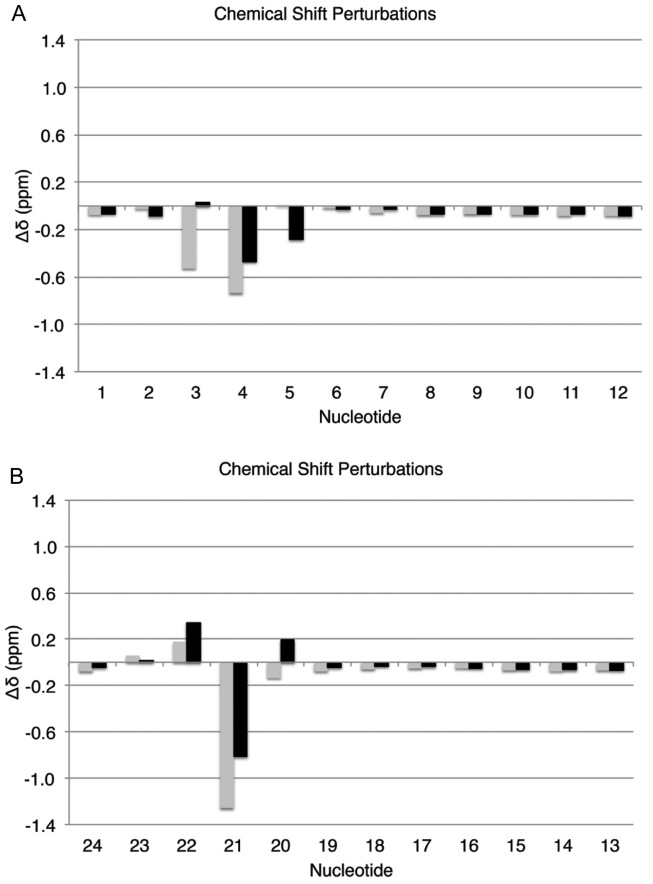

Figure 6. Chemical shift perturbations induced by the presence of the N^2-dG-IQ adduct at position G^1 of the *Nar*I restriction sequence. (A) The modified strand, showing nucleotides $C^1 \rightarrow C^{12}$. (B) The complementary strand, showing nucleotides $G^{24} \leftarrow G^{13}$. The black bars represent the deoxyribose H1′ resonances, and the gray bars represent the purine H8 or pyrimidine H6 resonances. In all cases, $\Delta\delta = \Delta\delta_{\text{unmodified}} - \Delta\delta_{\textit{Nar}\text{IQ at G}^1}$, where negative $\Delta\delta$ values correspond to downfield shifts and positive $\Delta\delta$ values correspond to upfield shifts.

Structure Refinement. Overall, a total of 283 NOEs were obtained from NOESY data (Table 2). Of these, 23 NOEs were involved in dipolar interactions between IQ and DNA protons. A total of 49 restraints for Watson−Crick hydrogen bonding were utilized, based upon the observation that the presence of the N^2-dG-IQ adduct prevented Watson−Crick hydrogen bonding only at the modified X^4:C^{21} base pair. No Watson−Crick hydrogen bonding restraint was applied at the X^4:C^{21} base pair. A total of 100 empirical phosphodiester backbone torsion angle restraints and 20 deoxyribose pseudorotation restraints based on canonical values for B-DNA[86] were also applied, based upon the observation that the structural perturbation to the DNA duplex was localized at the site of the lesion and the immediately flanking base pairs. These were not applied to base pairs C^3:G^{22}, X^4:C^{21}, and G^5:C^{20}. Ten emergent structures, based on the lowest deviations from experimental and empirical restraints, were selected. The convergence of these 10 structures is shown in Figure 7.

Table 2. Refinement Statistics for the N^2-dG-IQ at Position G^1 in the *Nar*I Sequence

NOE Restraints	
internucleotide	155
intranucleotide	128
total	283
backbone torsion angle restraints	100
H-bonding restraints	49
deoxyribose restraints	20
total number of restraints	442
Refinement Statistics	
number of distance restraint violations	70
number of torsion restraint violations	46
total distance penalty/maximum penalty [kcal mol^{-1}]	3.0/0.24
total torsion penalty/maximum penalty [kcal mol^{-1}]	1.7/0.16
RMS distances (Å)	0.012
RMS angles (deg)	2.5
distance restraint force field [kcal mol^{-1} $Å^{-2}$]	32
torsion restraint force field [kcal mol^{-1} deg^{-2}]	32

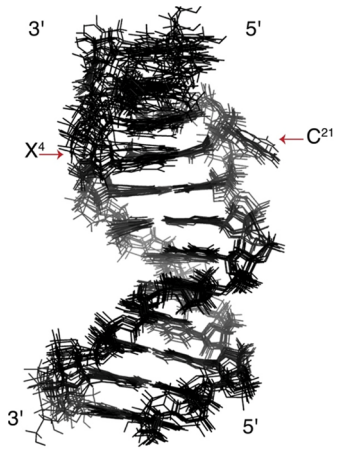

Figure 7. Superposition of the 10 structures emergent from the rMD calculations that exhibited the lowest deviations from experimental and empirical restraints. The arrows indicate the positions of the N^2-dG-IQ modified X^4 nucleotide and the complementary C^{21} nucleotide.

Table 3. Structural Statistics for the Refined Structure of the N^2-dG-IQ Adduct at Position G^1 in the *Nar*I Sequence

average structure (obtained from 10 structures)			
RMS pairwise difference between structures			1.27
RMS difference from average structure			0.85
complete relaxation matrix analysis analysis for average structure[a]			
	intranucleotide	internucleotide	total
R_x^{1} [b]	0.091	0.095	0.093
average error[c]			0.0037

[a]The mixing time was 150 ms. [b]R_1^x is the sixth root R factor: $\sum[((I_o)_i^{1/6} - (I_c)_i^{1/6})/\sum(I_o)_i^{1/6}]$. [c]Average error: $\sum(I_c - I_o)/n$, where the I_c is the NOE intensity calculated from the refined structure and I_o is the experimental NOE intensity.

Overall, these exhibited a maximum pairwise RMSD of 1.3 Å (Table 3). The rMD calculations exhibited poorer convergence at base pairs C^1:G^{24}, T^2:A^{23}, and C^3:G^{22}. This was attributed, in part, to the fraying of the duplex at the terminal base pairs.

These 10 structures were averaged and subjected to potential energy minimization, yielding an average structure. In the averaged structure, the total distance penalty was 3.0 kcal mol^{-1}, with the maximum individual distance penalty being 0.24 kcal mol^{-1}. The total torsion angle penalty was 1.7 kcal mol^{-1}, with the maximum single torsion angle penalty being

DOI: 10.1021/acs.chemrestox.5b00140
Chem. Res. Toxicol. 2015, 28, 1455−1468

0.16 kcal mol^{-1}. Complete relaxation matrix calculations were performed using the program CORMA to evaluate the agreement between the average structure and the NOE data. These showed that the overall sixth root residual (R_1^x value) for the average of the structures emergent from the rMD calcutions was 0.09. The sixth root residuals for the individual nucleotides (Figure 8) remained below 0.10, with the exception of

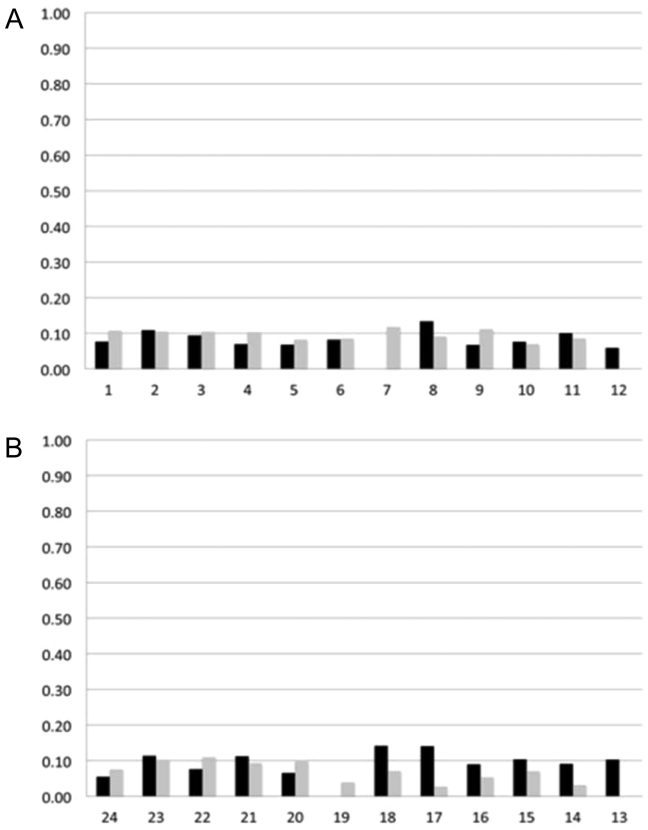

Figure 8. Sixth root residuals (R_1^x) obtained from complete relaxation matrix calculations from the average of 10 structures emergent from the rMD calculations of the N^2-dG-IQ modified duplex. The black bars represent intranucleotide sixth root residuals, and the gray bars represent internucleotide sixth root residuals. (A) Nucleotides C^1–C^{12} in the modified strand. (B) Nucleotides G^{13}–G^{24} in the complementary strand.

nucleotides C^8, G^{17}, and C^{18}, which remained below 0.15. However, nucleotides C^8, G^{17}, and C^{18} were each at least three nucleotides away from modified base pair X^4:C^{21}, and the greater sixth root residuals observed for these three nucleotides were attributed to less accurate measurements of distances due to spectral overlap involving these nucleotides.

Conformation of the N^2-dG-IQ Adduct. In the average refined structure (Figure 9), modified guanine base X^4 remained in the *anti* conformation about the glycosidic bond, but it shifted toward the major groove. The IQ ring was intercalated into the duplex. The complementary base C^{21} was displaced from the duplex and was into the major groove. The intercalated IQ ring was positioned such that the imidazole portion of the IQ ring, containing the CH_3 and H4a protons, oriented toward the modified strand of the duplex, whereas the quinoline moiety, containing the H7a, H8a, and H9a protons, oriented toward the complementary strand. The intercalated IQ moiety remained in-plane with damaged base X^4. The X^4 C2–

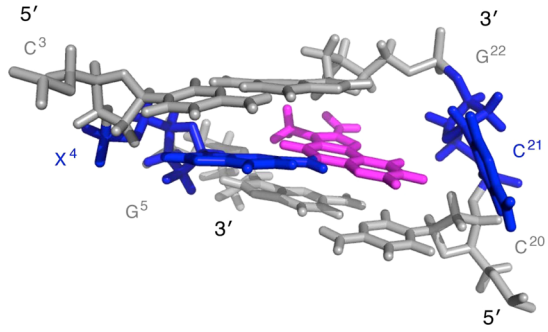

Figure 9. Expanded view of the average refined structure of the N^2-dG-IQ adduct located at position G^1 of the *Nar*I restriction sequence, showing base pairs C^3:G^{22}, X^4:C^{21}, and G^5:C^{20}, as shown from the major groove. The IQ moiety is in magenta.

X^4 N^2–IQ C5–IQ C6 dihedral angle was 178°. The stacking of the 5′-neighbor C^3:G^{22} base pair and of the 5′-neighbor base pair G^5:C^{20} relative to the modified X^4 base is shown in Figure 10. The IQ moiety was stacked primarily above the 3′-neighbor G^5:C^{20} base pair, with the X^4 guanine base stacked below the

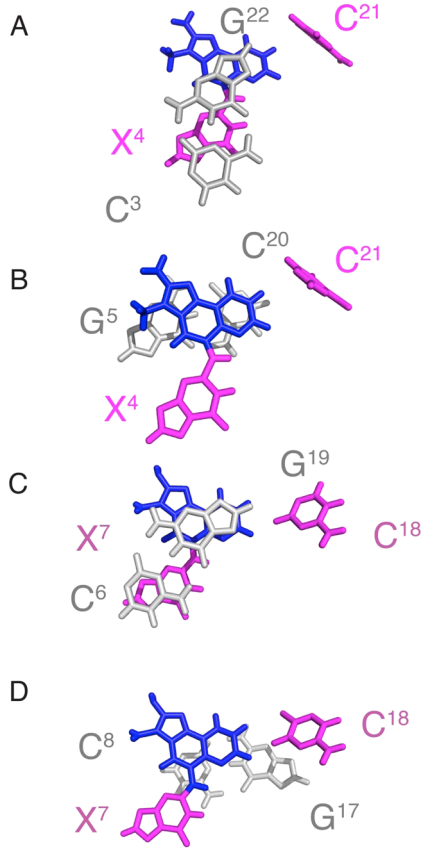

Figure 10. Expanded views of base-stacking interactions for the N^2-dG-IQ adduct located at position G^1 of the *Nar*I restriction sequence, as compared to the N^2-dG-IQ adduct located at position G^3 of the *Nar*I restriction sequence. (A) The N^2-dG-IQ adduct at position G^1. Stacking of base pair C^3:G^{22} above base pair X^4:C^{21}, with IQ shown in magenta. (B) The N^2-dG-IQ adduct at position G^1. Stacking of base pair X^4:C^{21} above base pair G^5:C^{20}. (C) The N^2-dG-IQ adduct at position G^3. Stacking of base pair C^6:G^{19} above base pair X^7:C^{18}, with IQ shown in magenta. (D) The N^2-dG-IQ adduct at position G^3. Stacking of base pair X^7:C^{18} above base pair C^8:G^{17}, with IQ shown in magenta.

DOI: 10.1021/acs.chemrestox.5b00140
Chem. Res. Toxicol. 2015, 28, 1455–1468

5′-neighbor C^3:G^{22} base pair. Helicoidal analysis indicated that accommodation of the IQ moiety in the duplex created a localized unwinding and conformational perturbation of the helix. The helical twist decreased by 15° at the adduction site. The tip of the 5′-neighbor base pair C^3:G^{22} increased by 20°. The tilt between C^3 and X^4 decreased by 13°, and between X^4 and G^5, it increased by 23°. The roll between bases C^3 and X^4 decreased by 24°, and that between X^4 and G^5 increased by 21°. The displacement of the complementary base C^{21} into the major groove was evidenced by a 98° increase in base opening as compared to the G^4:C^{21} base pair in the unmodified duplex. At the lesion site, the average structure of the modified duplex was bent 10° compared to the unmodified duplex.

DISCUSSION

IQ[1−5] is a genotoxic HCA food mutagen that is metabolized to an electrophilic nitrenium ion that alkylates guanines in DNA, forming both C8-dG-IQ and N^2-dG-IQ adducts.[26] It may play a significant role in cancer etiology.[18,19] Polymerase bypass studies conducted *in vitro* have revealed that the consequences of replication past the N^2-dG-IQ adduct differ when the lesion was incorporated[63,72] at position G^1 vs G^3 of the *Nar*I restriction endonuclease sequence, 5′-d($G^1G^2CG^3$CC)-3′.[66−71] Two-base deletions were produced by hpol η when the N^2-dG-IQ adduct was located at the G^3 position, but when this lesion was located at the G^1 position, error-free incorporation of dCTP occurred but further replication stalled.[72] Moreover, in bacteria, the genotoxicity of a number of aryl amine adducts depends upon the relative placement of these lesions, either at the nonreiterated G^1 position or the reiterated G^3 position within the *Nar*I sequence.[66−71] Consequently, the structural consequences of placing the N^2-dG-IQ adduct[51−53] at the G^1 vs G^3 position of the *Nar*I restriction sequence were of interest.

Base-Displaced Intercalated Conformation of the N^2-dG-IQ Adduct at Position G^1 in the *Nar*I Sequence. The present studies indicate that when the N^2-dG-IQ adduct is placed at the nonreiterated G^1 position in the *Nar*I restriction site it adopts a base-displaced intercalated conformation, in which modified base X^4 remains in the *anti* conformation with respect to the gycosidic torsion angle χ and the IQ heterocyclic ring intercalates and displaces the complementary base, C^{21}, into the major groove (Figure 9). The *anti* conformation of modified base X^4 is supported by the NOE between the X^4 H8 and X^4 H1′ protons (Figure 2), which is of similar intensity as those of the other purine H8 to H1′ NOEs. The positioning of the IQ aryl ring is defined by NOEs between the IQ adduct and DNA (Figure 5). The IQ CH_3 and H4a protons exhibit NOEs to X^4 and G^5 H1′, indicating that this portion of the IQ aryl ring faces the modified strand. NOEs between the IQ H7a, H8a, and H9a quinoline protons indicate that this portion of the aryl ring faces the complementary strand (Table 1). The intercalated IQ aryl ring stacks with the flanking base pairs C^3:G^{22} and G^5:C^{20} (Figure 10). The intercalation of the IQ moiety places the edge of the aryl ring containing the CH_3, H4a, H7a, H8a, and H9a faces into the minor groove. The chemical shifts of the H4a, H7a, H8a, and H9a IQ proton resonances range from 6.9−8.6 ppm (Table S3, Supporting Information). These values, 0.5−0.9 ppm upfield from their spectral positions in the corresponding N^2-dG-IQ nucleoside, indicate a shielding effect from the duplex. Likewise, the IQ CH_3 resonances shift upfield 0.4 ppm as compared to the N^2-dG-IQ nucleoside. In the refined structure, the CH_3 group faces into the minor groove, which may be consistent with the somewhat smaller upfield shift of the CH_3 resonance as compared to that of the H4a, H7a, H8a, and H9a IQ proton resonances. At the 3′-neighbor base pair G^5:C^{20}, the upfield shift of C^{20} H6 resonance (Figure 6) is likely due to stacking in the presence of the IQ aryl ring. In contrast, the downfield chemical shift change of 1.3 ppm for the C^{21} H6 resonance relative to C^{21} in the unmodified duplex reflects the displacement of C^{21} into the major groove. The downfield chemical shifts observed for the 5′-flanking base C^3 H6, X^4 H8, and 3′-flanking base G^5 H8 resonances (Figure 6) are difficult to interpret but presumably reflect the changes in shielding due to the base-displaced intercalated conformation of the N^2-dG-IQ adduct as compared to the normal Watson−Crick base pairing environment. At the lesion site, the X^4 N1H imino proton resonance is observed (Figure 3), indicating that its exchange with water is slow. Significantly, when the N^2-dG-IQ adduct was positioned at X^7 (G^3 in the *Nar*I sequence), the X^7 N1H imino proton resonance was also observed in spectra.[64] The sharp resonance at 9.5 ppm was assigned to the X^4 N^2H amino proton (Figure 3). This resonance remained sharp to a temperature of 55 °C, when most of the duplex is melted, suggesting that a stabilizing effect comes from an intrastrand interaction.

Despite the rather substantial conformational perturbation introduced into the duplex by the N^2-dG-IQ adduct (Figure 9), the thermal melting temperature is 62 °C, as compared to 63 °C for the unmodified sequence. The minimal effect of the N^2-dG-IQ adduct upon the thermal stability of the duplex is attributed to favorable stacking interactions with bases C^{20} and G^{22}, as shown in Figure 10, which evidently compensate for the loss of Watson−Crick hydrogen bonding at the modified base pair. Similar effects have been observed for N^6-dA adducts arising from alkylation by fjord-region dibenzo[*a*,*l*]pyrene diol epoxides, demonstrating the importance of base stacking to duplex stability.[98−100]

Similar Conformations of the N^2-dG-IQ Adduct at Both Positions G^1 and G^3 of the *Nar*I Restriction Site Sequence. Previously, the conformation of the N^2-dG-IQ adduct at the mutagenic hotspot, G^3, in the 5′-d(G^1G^2-CG^3CC)-3′[66−71] *Nar*I recognition sequence was determined.[64] The conformations of the N^2-dG-IQ adduct at these two positions in the *Nar*I sequence are similar, as can be observed in the stacking interactions shown in Figure 10. The CD spectra (Figure 1) confirm that the conformations of the N^2-dG-IQ adducts are similar when placed either at the G^1 or G^3 position of the *Nar*I sequence. Both modified sequences have a decrease in absorbance at the maximum wavelength (270 nm). The change in absorbance at this wavelength is likely related to DNA structure, particularly the average rotation between base pairs.[101] Therefore, the change in absorbance could correspond to an increase in the degrees per base pair of the duplex, but other secondary structures likely contribute to this change as well. A lack of a visible signal in both sequence contexts between 300 and 360 nm, where the IQ-induced signal should occur, could support that the conformation of the modified base adopts a similar conformation in both sequences, but this is inconclusive since the lack of signal could also be due to a reduction in the IQ chromophore from the linkage at dGuo N^2 to the IQ ring. When placed at the G^2 position in the *Nar*I sequence, the C8-AF-dG adduct exhibited a negative CD signal in the 300−360 nm range, which was assigned to the groove-bound conformation. In contrast, when placed at the G^1 or G^3 position of the *Nar*I sequence, a positive signal was observed

DOI: 10.1021/acs.chemrestox.5b00140
Chem. Res. Toxicol. 2015, 28, 1455−1468

for the C8-AF-dG adduct in the 300−360 nm range, which was assigned to the base-displaced intercalated conformation.[102]

There are subtle differences between the conformations of the N^2-dG-IQ adduct located at the G^1 vs G^3 position (Figure 10). This is perhaps due to the different nearest-neighbor sequence contexts for the two sites, 5′-$C^3X^4G^5C^{6\prime}$-3′ vs 5′-$C^6X^7C^8C^9$-3′, which differ in the 3′-flanking sequences. The modulation of both nucleotide excision repair and polymerase bypass of C8-dG arylamine adducts as a function of 3′-flanking sequence, attributed to differential conformational effects, including the orientation of base stacking, has been noted by Jain et al.[73−75] In the present instance, the G^1 N^2-dG-IQ adduct maintained planarity with the X^4 guanine base (Figure 9), but for the G^3 N^2-dG-IQ adduct, the IQ aryl ring was inserted at a 15° angle relative to the X^7 guanine base. In the G^1 sequence context (Figure 9), C^{21} rotated 20° further out of the duplex than did C^{18} in the G^3 sequence context. A similar effect on the helical twist between the 5′-neighbor base to the modified base was observed, which was reduced by 30°. However, the G^1 N^2-dG-IQ adduct showed greater unwinding of the duplex from the modified base to the 3′-neighbor, with an increase of 15° compared to the 9° increase for G^3 duplex. The blue shifts in the CD data correspond to adduct-induced twisting and/or bending for both duplexes (Figure 1). The chemical shifts of the IQ H7a and H9a protons in the G^1 vs G^3 sequence contexts are 0.45 and 0.3 ppm further downfield, respectively, for the G^1 position, whereas all of the other IQ ring protons differed by less than 0.1 ppm. The localized unwinding of the duplex for the N^2-dG-IQ adduct positioned at the G^1 site could be sufficient to alter base stacking orientations with the IQ heterocyclic ring and account for the chemical shift differences of these protons, although these small conformational changes are not reflected in the respective T_m values of the duplexes.

Structure−Activity Relationships. The ultimate carcinogen produced by IQ metabolism is a nitrenium ion (Scheme 1), which alkylates DNA. The N^2-dG-IQ adduct is the minor alkylaton product,[51−53] with the C8-dG-IQ adduct being the major product (Scheme 1). Nevertheless, in rat tissues, the N^2-dG-IQ adduct is more persistent than is the C8-dG-IQ adduct[59] and is anticipated to contribute more toward the genotoxic properties of IQ.[103] The relative thermal stability of the N^2-dG-IQ adduct as compared to the corresponding unmodified duplex was also noted when the lesion was placed at G^3 of the *Nar*I sequence.[64] The minimal effects of the N^2-dG-IQ adducts upon the T_m values of the duplexes may help to explain the relative persistence of this adduct in rat tissues.[59]

If it is not repaired, the N^2-dG-IQ adduct is mutagenic. Choi et al.[72] placed the N^2-dG-IQ adduct at either the G^1 or G^3 site of the *Nar*I sequence, in which the G^3 site is a hot spot for frameshift mutations in bacteria with the model arylamine derivative 2-acetylaminofluorene but G^1 is not.[67−69,71] Choi et al.[72] showed that primer extension by hpol η beyond template N^2-dG-IQ adducts was more efficient than that for hpol κ and much better than that for pol ι or δ. In single-base incorporation studies, hpol η correctly inserted dCTP and incorrectly inserted dATP, hpol ι incorrectly inserted dTTP, and hpol κ incorrectly inserted dGTP. Steady-state kinetic parameters were measured for these dNTPs opposite the N^2-dG-IQ adducts at both sites, being most favorable for hpol η. Mass spectrometric analyses of extension products arising from hpol η bypass revealed that a −2 deletion occurred for the N^2-dG-IQ adduct at the G^3 position. With the G^1 N^2-dG-IQ adduct, dCTP was correctly inserted, but further extension then stalled. Thus, hpol η products yielded frameshifts with the N^2-dG-IQ at the G^3 position but not at the G^1 position of the *Nar*I sequence.[72] The present studies, revealing that the base-displaced intercalated conformations of the N^2-dG-IQ adducts are similar at both the G^1 and G^3 positions of the *Nar*I sequence (Figure 10), do not readily explain the difference in bypass by hpol η at the two sites. It seems likely that the ability of the N^2-dG-IQ adduct to induce −2 base deletions at the G^3 site but not at the G^1 site must instead be determined by sequence-specific differences in the chemistry and structural biology of lesion bypass in the presence of hpol η, e.g., differences in abilities to form or to process slipped frameshift intermediates during lesion bypass, as has been proposed by Jain et al.[75,102] Again, the identities of the 3′-flanking sequences may be of importance in the stabilization of such enzyme-bound frameshift intermediates.[73−75] Studies to examine the details of specific interactions between the N^2-dG-IQ adduct at either the G^1 vs G^3 position, in the presence of pol η, will thus be of interest.

■ SUMMARY

N^2-dG-IQ assumes a base-displaced intercalated conformation when placed site specifically at the G^1 position in the *Nar*I restriction endonuclease sequence. The overall conformation is similar to that for the same adduct placed at the G^3 position. Consequently, we conclude that in the *Nar*I 5′-d(CG^1G^2-CG^3CC)-3′ restriction site the conformation of the N^2-dG-IQ adduct does not strongly depend upon sequence, although there are subtle differences in the base-displaced intercalated conformations at the G^1 vs G^3 position, which may be related to differences in the respective 3′-flanking sequences.[73−75] Moreover, at both positions G^1 and G^3, the N^2-dG-IQ adduct does not significantly reduce the T_m of the duplex,[64] which correlates with the observation that the N^2-dG-IQ adduct is less efficiently repaired in rat tissues[59] as compared to that for the C8-dG-IQ adduct, which does reduce the T_m of the duplex. This differs from the C8-dG-IQ adduct, the conformation of which is sensitive to sequence context in the *Nar*I restriction site. Nevertheless, the N^2-dG-IQ adduct is differentially processed by hpol η when placed at the G^1 vs G^3 position,[72] suggesting that replication bypass by hpol η may involve sequence-specific differences in the ability to form the enzyme-bound transient strand slippage intermediates that are associated with frameshift mutations.

■ ASSOCIATED CONTENT

Supporting Information

Tables S1: Comparative thermal melting temperatures (T_m) of IQ-, AF-, and AAF-modified oligodeoxynucleotides. Table S2: Chemical shift assignments (ppm) for the nonexchangeable DNA protons of the N^2-dG-IQ modified duplex at the G^1 position of the *Nar*I sequence. Table S3: Chemical shift assignments (ppm) for the exchangeable DNA protons of the N^2-dG-IQ modified duplex at the G^1 position of the *Nar*I sequence. Table S4: Chemical shift assignments for the IQ protons of the N^2-dG-IQ modified duplex at the G^1 position of the *Nar*I sequence. The Supporting Information is available free of charge on the ACS Publications website at DOI: 10.1021/acs.chemrestox.5b00140.

DOI: 10.1021/acs.chemrestox.5b00140
Chem. Res. Toxicol. 2015, 28, 1455−1468

Accession Codes

The structural coordinates were deposited in the Protein Data Bank (www.rcsb.org): the PDB ID code for the N^2-dG-IQ duplex is 2N0Q.

AUTHOR INFORMATION

Corresponding Author

*Telephone: 615-322-2589. E-mail: michael.p.stone@vanderbilt.edu.

Funding

This work was supported by the National Institutes of Health [R01 CA55678 to M.P.S., R01 ES016561 to C.J.R., Center Grants P30 ES000267 and P30 CA068485, and instrumentation grants S10 RR05805, S10 RR025677, and National Science Foundation instrumentation grant DBI 0922862, the latter of which was funded by the American Recovery and Reinvestment Act of 2009 (Public Law 111-5)]. Vanderbilt University assisted with the purchase of NMR instrumentation. K.M.S. and E.K.H. acknowledge support from National Institutes of Health training grant T32 ES007028. Funding for open access charge: National Institutes of Health.

Notes

The authors declare no competing financial interest.

‡Edward K. Hawkins is deceased.

ABBREVIATIONS

AAF, *N*-2-acetylaminofluorene; AF, 2-aminofluorene; B[*a*]P, benzo[a]pyrene; CD, circular dichroism; COSY, correlation spectroscopy; HCA, hetercyclic amine; HPLC, high-performance liquid chromatography; IQ, 2-amino-3-methylimidazo[4,5-*f*]quinoline; MALDI-TOF, matrix-assisted laser desorption time-of-flight mass spectrometry; NOESY, nuclear Overhauser effect spectroscopy; rMD, restrained molecular dynamics; PAH, polycyclic aromatic hydrocarbon; T_m, temperature at which the duplex DNA:single strand DNA is 1:1

REFERENCES

(1) Wakabayashi, K., Nagao, M., Esumi, H., and Sugimura, T. (1992) Food-derived mutagens and carcinogens. *Cancer Res. 52*, 2092s−2098s.

(2) Layton, D. W., Bogen, K. T., Knize, M. G., Hatch, F. T., Johnson, V. M., and Felton, J. S. (1995) Cancer risk of heterocyclic amines in cooked foods: an analysis and implications for research. *Carcinogenesis 16*, 39−52.

(3) Sugimura, T. (1997) Overview of carcinogenic heterocyclic amines. *Mutat. Res. 376*, 211−219.

(4) Sugimura, T., Wakabayashi, K., Nakagama, H., and Nagao, M. (2004) Heterocyclic amines: mutagens/carcinogens produced during cooking of meat and fish. *Cancer Sci. 95*, 290−299.

(5) Turesky, R. J., and Le Marchand, L. (2011) Metabolism and biomarkers of heterocyclic aromatic amines in molecular epidemiology studies: lessons learned from aromatic amines. *Chem. Res. Toxicol. 24*, 1169−1214.

(6) Kataoka, H., Nishioka, S., Kobayashi, M., Hanaoka, T., and Tsugane, S. (2002) Analysis of mutagenic heterocyclic amines in cooked food samples by gas chromatography with nitrogen-phosphorus detector. *Bull. Environ. Contam. Toxicol. 69*, 682−689.

(7) Felton, J. S., Knize, M. G., Salmon, C. P., Malfatti, M. A., and Kulp, K. S. (2002) Human exposure to heterocyclic amine food mutagens/carcinogens: relevance to breast cancer. *Environ. Mol. Mutagen. 39*, 112−118.

(8) Yamashita, M., Wakabayashi, K., Nagao, M., Sato, S., Yamaizumi, Z., Takahashi, M., Kinae, N., Tomita, I., and Sugimura, T. (1986) Detection of 2-amino-3-methylimidazo[4,5-*f*]quinoline in cigarette smoke condensate. *Jpn. J. Cancer Res. 77*, 419−422.

(9) Ohgaki, H., Hasegawa, H., Kato, T., Suenaga, M., Ubukata, M., Sato, S., Takayama, S., and Sugimura, T. (1986) Carcinogenicity in mice and rats of heterocyclic amines in cooked foods. *Environ. Health Perspect. 67*, 129−134.

(10) Adamson, R. H., Thorgeirsson, U. P., Snyderwine, E. G., Thorgeirsson, S. S., Reeves, J., Dalgard, D. W., Takayama, S., and Sugimura, T. (1990) Carcinogenicity of 2-amino-3-methylimidazo[4,5-*f*]quinoline in nonhuman primates: Induction of tumors in three macaques. *Jpn. J. Cancer Res. 81*, 10−14.

(11) Heflich, R. H., and Neft, R. E. (1994) Genetic toxicity of 2-acetylaminofluorene, 2-aminofluorene and some of their metabolites and model metabolites. *Mutat. Res. 318*, 73−114.

(12) Thorgeirsson, U. P., Snyderwine, E. G., Gomez, D. E., and Adamson, R. H. (1996) Dietary heterocyclic amines as potential human carcinogens: experimental data from nonhuman primates. *In Vivo 10*, 145−152.

(13) Ohgaki, H., Kusama, K., Matsukura, N., Morino, K., Hasegawa, H., Sato, S., Takayama, S., and Sugimura, T. (1984) Carcinogenicity in mice of a mutagenic compound, 2-amino-3-methylimidazo[4,5-*f*]-quinoline, from broiled sardine, cooked beef and beef extract. *Carcinogenesis 5*, 921−924.

(14) Takayama, S., Nakatsuru, Y., Masuda, M., Ohgaki, H., Sato, S., and Sugimura, T. (1984) Demonstration of carcinogenicity in F344 rats of 2-amino-3-methyl-imidazo[4,5-*f*]quinoline from broiled sardine, fried beef and beef extract. *Gann 75*, 467−470.

(15) Tanaka, T., Barnes, W. S., Williams, G. M., and Weisburger, J. H. (1985) Multipotential carcinogenicity of the fried food mutagen 2-amino-3-methylimidazo[4,5-*f*]quinoline in rats. *Jpn. J. Cancer Res. 76*, 570−576.

(16) Sugimura, T., Nagao, M., and Wakabayashi, K. (2000) in *Complex Factors Pertinent to Human Hazard and Risk*, pp 349−359, Wiley, New York.

(17) Kobayashi, M., Hanaoka, T., Nishioka, S., Kataoka, H., and Tsugane, S. (2002) Estimation of dietary HCA intakes in a large-scale population-based prospective study in Japan. *Mutat. Res. 506−507*, 233−241.

(18) (1993) *IARC Monographs on the Evaluation of Carcinogenic Risks to Humans*, Vol. *56*, International Agency for Research on Cancer, Lyon, France.

(19) (2005) *Report on Carcinogenesis*, 11th ed., National Toxicology Program, Research Triangle Park, NC.

(20) Anderson, K. E., Hammons, G. J., Kadlubar, F. F., Potter, J. D., Kaderlik, K. R., Ilett, K. F., Minchin, R. F., Teitel, C. H., Chou, H. C., Martin, M. V., Guengerich, F. P., Barone, G. W., Lang, N. P., and Peterson, L. A. (1997) Metabolic activation of aromatic amines by human pancreas. *Carcinogenesis 18*, 1085−1092.

(21) Lang, N. P., Butler, M. A., Massengill, J., Lawson, M., Stotts, R. C., Hauer-Jensen, M., and Kadlubar, F. F. (1994) Rapid metabolic phenotypes for acetyltransferase and cytochrome P4501A2 and putative exposure to food-borne heterocyclic amines increase the risk for colorectal cancer or polyps. *Cancer Epidemiol., Biomarkers Prev. 3*, 675−682.

(22) Shirai, T., Sano, M., Tamano, S., Takahashi, S., Hirose, M., Futakuchi, M., Hasegawa, R., Imaida, K., Matsumoto, K., Wakabayashi, K., Sugimura, T., and Ito, N. (1997) The prostate: A target for carcinogenicity of 2-amino-1-methyl-6-phenylimidazo[4,5-*b*]pyridine (PhIP) derived from cooked foods. *Cancer Res. 57*, 195−198.

(23) Snyderwine, E. G. (1994) Some perspectives on the nutritional aspects of breast cancer research. Food-derived heterocyclic amines as etiologic agents in human mammary cancer. *Cancer 74*, 1070−1077.

(24) Ronco, A., De Stefani, E., Mendilaharsu, M., and Deneo-Pellegrini, H. (1996) Meat, fat and risk of breast cancer: a case-control study from Uruguay. *Int. J. Cancer 65*, 328−331.

(25) Ushiyama, H., Wakabayashi, K., Hirose, M., Itoh, H., Sugimura, T., and Nagao, M. (1991) Presence of carcinogenic heterocyclic amines in urine of healthy volunteers eating normal diet, but not of inpatients receiving parenteral alimentation. *Carcinogenesis 12*, 1417−1422.

DOI: 10.1021/acs.chemrestox.5b00140
Chem. Res. Toxicol. 2015, 28, 1455−1468

(26) Sugimura, T., and Sato, S. (1983) Mutagens-carcinogens in foods. *Cancer Res. 43*, 2415s−2421s.
(27) Nagao, M. (2000). In *Food-Borne Carcinogens: Heterocyclic Amines* (Nagao, M., and Sugimura, T., Eds.) pp 31−71, Wiley, New York.
(28) Hecht, S. S. (2002) Tobacco smoke carcinogens and breast cancer. *Environ. Mol. Mutagen. 39*, 119−126.
(29) Kosakarn, P., Halliday, J. A., Glickman, B. W., and Josephy, P. D. (1993) Mutational specificity of 2-nitro-3,4-dimethylimidazo[4,5-*f*] quinoline in the lacI gene of *Escherichia coli*. *Carcinogenesis 14*, 511−517.
(30) Watanabe, M., and Ohta, T. (1993) Analysis of mutational specificity induced by heterocyclic amines in the *lac*Z gene of *Escherichia coli*. *Carcinogenesis 14*, 1149−1153.
(31) Terada, M., Nagao, M., Nakayasu, M., Sakamoto, H., Nakasato, F., and Sugimura, T. (1986) Mutagenic activities of heterocyclic amines in Chinese hamster lung cells in culture. *Environ. Health Perspect. 67*, 117−119.
(32) Thompson, L. H., Tucker, J. D., Stewart, S. A., Christensen, M. L., Salazar, E. P., Carrano, A. V., and Felton, J. S. (1987) Genotoxicity of compounds from cooked beef in repair-deficient CHO cells versus Salmonella mutagenicity. *Mutagenesis 2*, 483−487.
(33) Felton, J. S., Fultz, E., Dolbeare, F. A., and Knize, M. G. (1994) Effect of microwave pretreatment on heterocyclic aromatic amine mutagens/carcinogens in fried beef patties. *Food Chem. Toxicol. 32*, 897−903.
(34) Schut, H. A., and Snyderwine, E. G. (1999) DNA adducts of heterocyclic amine food mutagens: implications for mutagenesis and carcinogenesis. *Carcinogenesis 20*, 353−368.
(35) Turesky, R. J. (2002) Heterocyclic aromatic amine metabolism, DNA adduct formation, mutagenesis, and carcinogenesis. *Drug Metab. Rev. 34*, 625−650.
(36) Thompson, L. H., Carrano, A. V., Salazar, E., Felton, J. S., and Hatch, F. T. (1983) Comparative genotoxic effects of the cooked-food-related mutagens Trp-P-2 and IQ in bacteria and cultured mammalian cells. *Mutat. Res. 117*, 243−257.
(37) Aeschbacher, H. U., and Ruch, E. (1989) Effect of heterocyclic amines and beef extract on chromosome aberrations and sister chromatid exchanges in cultured human lymphocytes. *Carcinogenesis 10*, 429−433.
(38) Tohda, H., Oikawa, A., Kawachi, T., and Sugimura, T. (1980) Induction of sister-chromatid exchanges by mutagens from amino acid and protein pyrolysates. *Mutat. Res. 77*, 65−69.
(39) Yamazoe, Y., Shimada, M., Kamataki, T., and Kato, R. (1983) Microsomal activation of 2-amino-3-methylimidazo[4,5-*f*]quinoline, a pyrolysate of sardine and beef extracts, to a mutagenic intermediate. *Cancer Res. 43*, 5768−5774.
(40) Boobis, A. R., Lynch, A. M., Murray, S., de la Torre, R., Solans, A., Farre, M., Segura, J., Gooderham, N. J., and Davies, D. S. (1994) CYP1A2-catalyzed conversion of dietary heterocyclic amines to their proximate carcinogens is their major route of metabolism in humans. *Cancer Res. 54*, 89−94.
(41) Shimada, T., Hayes, C. L., Yamazaki, H., Amin, S., Hecht, S. S., Guengerich, F. P., and Sutter, T. R. (1996) Activation of chemically diverse procarcinogens by human cytochrome P-450 1B1. *Cancer Res. 56*, 2979−2984.
(42) Hammons, G. J., Milton, D., Stepps, K., Guengerich, F. P., Tukey, R. H., and Kadlubar, F. F. (1997) Metabolism of carcinogenic heterocyclic and aromatic amines by recombinant human cytochrome P450 enzymes. *Carcinogenesis 18*, 851−854.
(43) Turesky, R. J., Constable, A., Richoz, J., Varga, N., Markovic, J., Martin, M. V., and Guengerich, F. P. (1998) Activation of heterocyclic aromatic amines by rat and human liver microsomes and by purified rat and human cytochrome P450 1A2. *Chem. Res. Toxicol. 11*, 925−936.
(44) Guengerich, F. P. (2002) N-hydroxyarylamines. *Drug Metab. Rev. 34*, 607−623.
(45) Minchin, R. F., Reeves, P. T., Teitel, C. H., McManus, M. E., Mojarrabi, B., Ilett, K. F., and Kadlubar, F. F. (1992) N-and O-acetylation of aromatic and heterocyclic amine carcinogens by human monomorphic and polymorphic acetyltransferases expressed in COS-1 cells. *Biochem. Biophys. Res. Commun. 185*, 839−844.
(46) Hein, D. W., Doll, M. A., Rustan, T. D., Gray, K., Feng, Y., Ferguson, R. J., and Grant, D. M. (1993) Metabolic activation and deactivation of arylamine carcinogens by recombinant human NAT1 and polymorphic NAT2 acetyltransferases. *Carcinogenesis 14*, 1633−1638.
(47) Hickman, D., Pope, J., Patil, S. D., Fakis, G., Smelt, V., Stanley, L. A., Payton, M., Unadkat, J. D., and Sim, E. (1998) Expression of arylamine N-acetyltransferase in human intestine. *Gut 42*, 402−409.
(48) Le Marchand, L., Hankin, J. H., Pierce, L. M., Sinha, R., Nerurkar, P. V., Franke, A. A., Wilkens, L. R., Kolonel, L. N., Donlon, T., Seifried, A., Custer, L. J., Lum-Jones, A., and Chang, W. (2002) Well-done red meat, metabolic phenotypes and colorectal cancer in Hawaii. *Mutat. Res. 506−507*, 205−214.
(49) Ishibe, N., Sinha, R., Hein, D. W., Kulldorff, M., Strickland, P., Fretland, A. J., Chow, W. H., Kadlubar, F. F., Lang, N. P., and Rothman, N. (2002) Genetic polymorphisms in heterocyclic amine metabolism and risk of colorectal adenomas. *Pharmacogenetics 12*, 145−150.
(50) Metry, K. J., Neale, J. R., Doll, M. A., Howarth, A. L., States, J. C., McGregor, W. G., Pierce, W. M., Jr., and Hein, D. W. (2010) Effect of rapid human N-acetyltransferase 2 haplotype on DNA damage and mutagenesis induced by 2-amino-3-methylimidazo-[4,5-*f*]quinoline (IQ) and 2-amino-3,8-dimethylimidazo-[4,5-*f*]quinoxaline (MeIQx). *Mutat. Res. 684*, 66−73.
(51) Snyderwine, E. G., Roller, P. P., Adamson, R. H., Sato, S., and Thorgeirsson, S. S. (1988) Reaction of N-hydroxylamine and N-acetoxy derivatives of 2-amino-3-methylimidazolo[4,5-*f*]quinoline with DNA. Synthesis and identification of N-(deoxyguanosin-8-yl)-IQ. *Carcinogenesis 9*, 1061−1065.
(52) Nagaoka, H., Wakabayashi, K., Kim, S. B., Kim, I. S., Tanaka, Y., Ochiai, M., Tada, A., Nukaya, H., Sugimura, T., and Nagao, M. (1992) Adduct formation at C-8 of guanine on *in vitro* reaction of the ultimate form of 2-amino-1-methyl-6-phenylimidazo[4,5-*b*]pyridine with 2′-deoxyguanosine and its phosphate esters. *Jpn. J. Cancer Res. 83*, 1025−1029.
(53) Turesky, R. J., Rossi, S. C., Welti, D. H., Lay, J. O., Jr., and Kadlubar, F. F. (1992) Characterization of DNA adducts formed in vitro by reaction of N-hydroxy-2-amino-3-methylimidazo[4,5-*f*]quinoline and N-hydroxy-2-amino-3,8-dimethylimidazo[4,5-*f*]quinoxaline at the C-8 and N^2 atoms of guanine. *Chem. Res. Toxicol. 5*, 479−490.
(54) Zenser, T. V., Lakshmi, V. M., Schut, H. A., Zhou, H. J., and Josephy, P. (2009) Activation of aminoimidazole carcinogens by nitrosation: mutagenicity and nucleotide adducts. *Mutat. Res. 673*, 109−115.
(55) Murata, M., and Kawanishi, S. (2011) Mechanisms of oxidative DNA damage induced by carcinogenic arylamines. *Front. Biosci., Landmark Ed. 16*, 1132−1143.
(56) Gangl, E. T., Turesky, R. J., and Vouros, P. (2001) Detection of *in vivo* formed DNA adducts at the part-per-billion level by capillary liquid chromatography/microelectrospray mass spectrometry. *Anal. Chem. 73*, 2397−2404.
(57) Soglia, J. R., Turesky, R. J., Paehler, A., and Vouros, P. (2001) Quantification of the heterocyclic aromatic amine DNA adduct N-(deoxyguanosin-8-yl)-2-amino-3-methylimidazo[4,5-*f*]quinoline in livers of rats using capillary liquid chromatography/microelectrospray mass spectrometry: a dose−response study. *Anal. Chem. 73*, 2819−2827.
(58) Nauwelaers, G., Bessette, E. E., Gu, D., Tang, Y., Rageul, J., Fessard, V., Yuan, J. M., Yu, M. C., Langouet, S., and Turesky, R. J. (2011) DNA adduct formation of 4-aminobiphenyl and heterocyclic aromatic amines in human hepatocytes. *Chem. Res. Toxicol. 24*, 913−925.
(59) Turesky, R. J., Markovic, J., and Aeschlimann, J. M. (1996) Formation and differential removal of C-8 and N2-guanine adducts of the food carcinogen 2-amino-3-methylimidazo[4,5-*f*]quinoline in the

DOI: 10.1021/acs.chemrestox.5b00140
Chem. Res. Toxicol. 2015, 28, 1455−1468

liver, kidney, and colorectum of the rat. *Chem. Res. Toxicol. 9*, 397−402.
(60) Wang, Z., and Rizzo, C. J. (2001) Synthesis of the C8-deoxyguanosine adduct of the food mutagen IQ. *Org. Lett. 3*, 565−568.
(61) Elmquist, C. E., Stover, J. S., Wang, Z., and Rizzo, C. J. (2004) Site-specific synthesis and properties of oligonucleotides containing C8-deoxyguanosine adducts of the dietary mutagen IQ. *J. Am. Chem. Soc. 126*, 11189−11201.
(62) Stover, J. S., and Rizzo, C. J. (2004) Synthesis of the N^2-deoxyguanosine adduct of the potent dietary mutagen IQ. *Org. Lett. 6*, 4985−4988.
(63) Stover, J. S., and Rizzo, C. J. (2007) Synthesis of oligonucleotides containing the N^2-deoxyguanosine adduct of the dietary carcinogen 2-amino-3-methylimidazo[4,5-*f*]quinoline. *Chem. Res. Toxicol. 20*, 1972−1979.
(64) Stavros, K. M., Hawkins, E. K., Rizzo, C. J., and Stone, M. P. (2014) Base-displaced intercalation of the 2-amino-3-methylimidazo-[4,5-f]quinolone N2-dG adduct in the NarI DNA recognition sequence. *Nucleic Acids Res. 42*, 3450−3463.
(65) Wang, F., Demuro, N. E., Elmquist, C. E., Stover, J. S., Rizzo, C. J., and Stone, M. P. (2006) Base-displaced intercalated structure of the food mutagen 2-amino-3-methylimidazo[4,5-*f*]quinoline in the recognition sequence of the *NarI* restriction enzyme, a hottspot for −2 bp deletions. *J. Am. Chem. Soc. 128*, 10085−10095.
(66) Fuchs, R. P., Schwartz, N., and Daune, M. P. (1981) Hot spots of frameshift mutations induced by the ultimate carcinogen N-acetoxy-N-2-acetylaminofluorene. *Nature 294*, 657−659.
(67) Koffel-Schwartz, N., Verdier, J. M., Bichara, M., Freund, A. M., Daune, M. P., and Fuchs, R. P. P. (1984) Carcinogen-induced mutation spectrum in wild-type, *uvrA* and *umuC* strains of *Escherichia coli*. *J. Mol. Biol. 177*, 33−51.
(68) Koehl, P., Burnouf, D., and Fuchs, R. P. P. (1989) Construction of plasmids containing a unique acetylaminofluorene adduct located within a mutation hot spot. A new probe for frameshift mutagenesis. *J. Mol. Biol. 207*, 355−364.
(69) Koehl, P., Valladier, P., Lefevre, J. F., and Fuchs, R. P. (1989) Strong structural effect of the position of a single acetylaminofluorene adduct within a mutation hot spot. *Nucleic Acids Res. 17*, 9531−9541.
(70) Hoffmann, G. R., and Fuchs, R. P. (1997) Mechanisms of frameshift mutations: insight from aromatic amines. *Chem. Res. Toxicol. 10*, 347−359.
(71) Broschard, T. H., Koffel-Schwartz, N., and Fuchs, R. P. (1999) Sequence-dependent modulation of frameshift mutagenesis at *Nar*I-derived mutation hot spots. *J. Mol. Biol. 288*, 191−199.
(72) Choi, J. Y., Stover, J. S., Angel, K. C., Chowdhury, G., Rizzo, C. J., and Guengerich, F. P. (2006) Biochemical basis of genotoxicity of heterocyclic arylamine food mutagens: human DNA polymerase eta selectively produces a two-base deletion in copying the N^2-guanyl adduct of 2-amino-3-methylimidazo[4,5-*f*]quinoline but not the C8 adduct at the *Nar*I G^3 site. *J. Biol. Chem. 281*, 25297−25306.
(73) Jain, V., Hilton, B., Patnaik, S., Zou, Y., Chiarelli, M. P., and Cho, B. P. (2012) Conformational and thermodynamic properties modulate the nucleotide excision repair of 2-aminofluorene and 2-acetylaminofluorene dG adducts in the NarI sequence. *Nucleic Acids Res. 40*, 3939−3951.
(74) Jain, V., Hilton, B., Lin, B., Patnaik, S., Liang, F., Darian, E., Zou, Y., Mackerell, A. D., Jr., and Cho, B. P. (2013) Unusual sequence effects on nucleotide excision repair of arylamine lesions: DNA bending/distortion as a primary recognition factor. *Nucleic Acids Res. 41*, 869−880.
(75) Jain, V., Vaidyanathan, V. G., Patnaik, S., Gopal, S., and Cho, B. P. (2014) Conformational insights into the lesion and sequence effects for arylamine-induced translesion DNA synthesis: ^{19}F NMR, surface plasmon resonance, and primer kinetic studies. *Biochemistry 53*, 4059−4071.
(76) Wang, F., Elmquist, C. E., Stover, J. S., Rizzo, C. J., and Stone, M. P. (2007) DNA sequence modulates the conformation of the food mutagen 2-amino-3-methylimidazo[4,5-*f*]quinoline in the recognition sequence of the *Nar*I restriction enzyme. *Biochemistry 46*, 8498−8516.
(77) Bodenhausen, G., Wagner, G., Rance, M., Sorensen, O. W., Wuthrich, K., and Ernst, R. R. (1984) Longitudinal two-spin order in 2D exchange spectroscopy (NOESY). *J. Magn. Reson. 59*, 542−550.
(78) Piotto, M., Saudek, V., and Sklenar, V. (1992) Gradient-tailored excitation for single-quantum NMR spectroscopy of aqueous solutions. *J. Biomol. NMR 6*, 661−665.
(79) Goddard, T. D., and Kneller, D. G. (2006) *SPARKY*, v. 3.113, University of California, San Francisco, CA.
(80) Keepers, J. W., and James, T. L. (1984) A theoretical study of distance determination from NMR. Two-dimensional nuclear Overhauser effect spectra. *J. Magn. Reson. 57*, 404−426.
(81) James, T. L. (1991) Relaxation matrix analysis of two-dimensional nuclear Overhauser effect spectra. *Curr. Opin. Struct. Biol. 1*, 1042−1053.
(82) Borgias, B. A., and James, T. L. (1989) Two-dimensional nuclear Overhauser effect: complete relaxation matrix analysis. *Methods Enzymol. 176*, 169−183.
(83) Borgias, B. A., and James, T. L. (1990) MARDIGRAS—a procedure for matrix analysis of relaxation for discerning geometry of an aqueous structure. *J. Magn. Reson. 87*, 475−487.
(84) Liu, H., Spielmann, H. P., Ulyanov, N. B., Wemmer, D. E., and James, T. L. (1995) Interproton distance bounds from 2D NOE intensities: Effect of experimental noise and peak integration errors. *J. Biomol. NMR 6*, 390−402.
(85) Spielmann, H. P., Dwyer, T. J., Hearst, J. E., and Wemmer, D. E. (1995) Solution structures of psoralen monoadducted and cross-linked DNA oligomers by NMR spectroscopy and restrained molecular dynamics. *Biochemistry 34*, 12937−12953.
(86) Arnott, S., and Hukins, D. W. L. (1972) Optimised parameters for A-DNA and B-DNA. *Biochem. Biophys. Res. Commun. 47*, 1504−1509.
(87) Frisch, M. J., Trucks, G. W., Schlegel, H. B., Scuseria, G. E., Robb, M. A., Cheeseman, J. R., Montgomery, J. A., Vreven, T., Kudin, K. N., Burant, J. C., Millam, J. M., Iyengar, S. S., Tomasi, J., Barone, V., Mennucci, B., Cossi, M., Scalmani, G., Rega, N., Petersson, G. A., Nakatsuji, H., Hada, M., Ehara, M., Toyota, K., Fukuda, R., Hasegawa, J., Ishida, M., Nakajima, T., Honda, Y., Kitao, O., Nakai, H., Klene, M., Li, X., Knox, J. E., Hratchian, H. P., Cross, J. B., Adamo, C., Jaramillo, J., Gomperts, R., Stratmann, R. E., Yazyev, O., Austin, A. J., Cammi, R., Pomelli, C., Pomelli, J., Ochterski, W., Ayala, P. Y., Morokuma, K., Voth, G. A., Salvador, P., Dannenberg, J. J., Zakrzewska, V. G., Daniels, A. D., Farkas, O., Rabuck, A. D., Raghavachari, K., and Ortiz, J. V. (2004) *Gaussian 03*, Gaussian, Inc., Wallingford, CT.
(88) Bashford, D., and Case, D. A. (2000) Generalized Born models of macromolecular solvation effects. *Annu. Rev. Phys. Chem. 51*, 129−152.
(89) Tsui, V., and Case, D. A. (2000) Theory and applications of the generalized Born solvation model in macromolecular simulations. *Biopolymers 56*, 275−291.
(90) Case, D. A., Cheatham, T. E., III, Darden, T., Gohlke, H., Luo, R., Merz, K. M., Jr., Onufriev, A., Simmerling, C., Wang, B., and Woods, R. J. (2005) The AMBER biomolecular simulation programs. *J. Comput. Chem. 26*, 1668−1688.
(91) Wang, J. M., Cieplak, P., and Kollman, P. A. (2000) How well does a restrained electrostatic potential (RESP) model perform in calculating conformational energies of organic and biological molecules? *J. Comput. Chem. 21*, 1049−1074.
(92) Kirkpatrick, S., Gelatt, C. D., Jr., and Vecchi, M. P. (1983) Optimization by simulated annealing. *Science 220*, 671−680.
(93) Lavery, R., Moakher, M., Maddocks, J. H., Petkeviciute, D., and Zakrzewska, K. (2009) Conformational analysis of nucleic acids revisited: Curves+. *Nucleic Acids Res. 37*, 5917−5929.
(94) Blanchet, C., Pasi, M., Zakrzewska, K., and Lavery, R. (2011) CURVES+ web server for analyzing and visualizing the helical, backbone and groove parameters of nucleic acid structures. *Nucleic Acids Res. 39*, W68−73.
(95) Patel, D. J., Shapiro, L., and Hare, D. (1987) DNA and RNA: NMR studies of conformations and dynamics in solution. *Q. Rev. Biophys. 20*, 35−112.

DOI: 10.1021/acs.chemrestox.5b00140
Chem. Res. Toxicol. 2015, 28, 1455−1468

(96) Reid, B. R. (1987) Sequence-specific assignments and their use in NMR studies of DNA structure. *Q. Rev. Biophys. 20*, 2−28.
(97) Elmquist, C. E., Wang, F., Stover, J. S., Stone, M. P., and Rizzo, C. J. (2007) Conformational differences of the C8-deoxyguanosine adduct of 2-amino-3-methylimidazo[4,5-*f*]quinoline (IQ) within the NarI recognition sequence. *Chem. Res. Toxicol. 20*, 445−454.
(98) Ruan, Q., Kolbanovskiy, A., Zhuang, P., Chen, J., Krzeminski, J., Amin, S., and Geacintov, N. E. (2002) Synthesis and characterization of site-specific and stereoisomeric fjord dibenzo[*a*,*l*]pyrene diol epoxide-N^6-adenine adducts: unusual thermal stabilization of modified DNA duplexes. *Chem. Res. Toxicol. 15*, 249−261.
(99) Reeves, D. A., Mu, H., Kropachev, K., Cai, Y., Ding, S., Kolbanovskiy, A., Kolbanovskiy, M., Chen, Y., Krzeminski, J., Amin, S., Patel, D. J., Broyde, S., and Geacintov, N. E. (2011) Resistance of bulky DNA lesions to nucleotide excision repair can result from extensive aromatic lesion-base stacking interactions. *Nucleic Acids Res. 39*, 8752−8764.
(100) Kropachev, K., Kolbanovskiy, M., Liu, Z., Cai, Y., Zhang, L., Schwaid, A. G., Kolbanovskiy, A., Ding, S., Amin, S., Broyde, S., and Geacintov, N. E. (2013) Adenine-DNA adducts derived from the highly tumorigenic dibenzo[*a*,*l*]pyrene are resistant to nucleotide excision repair while guanine adducts are not. *Chem. Res. Toxicol. 26*, 783−793.
(101) Baase, W. A., and Johnson, W. C., Jr. (1979) Circular dichroism and DNA secondary structure. *Nucleic Acids Res. 6*, 797−814.
(102) Jain, N., Li, Y., Zhang, L., Meneni, S. R., and Cho, B. P. (2007) Probing the sequence effects on NarI-induced −2 frameshift mutagenesis by dynamic ^{19}F NMR, UV, and CD spectroscopy. *Biochemistry 46*, 13310−13321.
(103) Poirier, M. C., and Beland, F. A. (1992) DNA adduct measurements and tumor incidence during chronic carcinogen exposure in animal models: implications for DNA adduct-based human cancer risk assessment. *Chem. Res. Toxicol. 5*, 749−755.

DOI: 10.1021/acs.chemrestox.5b00140
Chem. Res. Toxicol. 2015, 28, 1455−1468